Available online at www.sciencedirect.com
SCIENCE DIRECT®
International Journal of Heat and Mass Transfer 49 (2006) 1350–1357
International Journal of HEAT and MASS TRANSFER
www.elsevier.com/locate/ijhmt

Development of the film-splitting look-up table applicable to mechanistic annular film dryout model in annulus geometry

Ji-Han Chun [a,*], Won-Jae Lee [b,1], Un-Chul Lee [c,2]

[a] School of Materials, Mechanical, and Automation Engineering, Yanbian University of Science and Technology, Beishan St., Yanji City, Jilin Prov., 133000, China
[b] TH Safety Research Team, Korea Atomic Energy Research Institute, 150, Dukjin-dong, Yusung, Daejon 305-353, Korea
[c] Department of Nuclear Engineering, Seoul National University, San 56-1, Shinlim-dong, Gwanak, Seoul 151-742, Korea

Received 20 May 2004; received in revised form 30 September 2005
Available online 1 December 2005

Abstract

Annular flow in annulus geometry is characterized as two liquid films flowing along the inner heated rod and outer unheated wall. Critical heat flux (CHF) occurs when the liquid film on the inner heated wall dries out, while there still exists the liquid film on the outer cold wall. In the safety analysis code, film dryout is calculated by a mechanistic model or CHF table look-up method. The mechanistic film dryout is a complex function of film flow rate, applied heat flux and entrainment/deposition rate, etc. and is determined by the hydrodynamic solution. However, both models were not able to distinguish the liquid films on the cold surface from that on the hot surfaces in a calculation cell, that is, the cold wall effect. This resulted in over-estimation of the calculated CHF in the single-channel modeling of annulus geometry, so it needs a new model that could consider the cold wall effect mechanistically in the single-channel modeling. In order to consider the cold wall effect, a mechanistic film-splitting model look-up table was developed, in which the inner and outer liquid film fractions are solved analytically. The new look-up table was assessed using Wurtz experimental data and was assessed indirectly using several annulus geometry CHF test data.

Keywords: Annular film dryout; Annulus geometry; Film-splitting; Cold wall effect; Critical heat flux

1. Introduction

CHF (critical heat flux) is defined as a discontinuous reduction of the local heat transfer coefficient, which results from the replacement of liquid by vapor on a heated surface. To understand this phenomenon is very important in the nuclear reactor safety, because the fuel failure due to a rapid heat-up by CHF in a short time can lead the release of radioactive materials into environments.

CHF phenomenon is considered in two kinds of mechanisms. One is called as the Departure of Nucleate Boiling (DNB), in which the vapor blanket covering the heated surface deteriorates the heat transfer rate. Heat transfer regime transits from subcooled or saturated nucleate boiling to film boiling. DNB occurs when the surface heat flux is relatively high and the void quality is low and it has been the major safety concern of pressurized water reactor (PWR) transients. Another mechanism is the annular film dryout, in which a continuous liquid film on the heated surface is dried out by droplet entrainment and evaporation. The dryout mechanism has been the main safety concern not only of the boiling water reactor transients but also of the PWR transients. Dryout occurs in an annular flow regime when the void quality is relatively high.

Most of the thermal-hydraulic transient codes for PWRs use a CHF look-up table method or experimental CHF correlations specific to fuel design. Since DNB has been the major safety issue of PWR safety, there are a lot of

* Corresponding author. Tel.: +86 433 291 2978.
E-mail addresses: jhchun@ybust.edu.cn (J.-H. Chun), wjlee@kaeri.re.kr (W.-J. Lee), uclee@snu.ac.kr (U.-C. Lee).
[1] Tel.: +82 42 868 2980.
[2] Tel.: +82 2 880 7206.

0017-9310/$ - see front matter © 2005 Elsevier Ltd. All rights reserved.
doi:10.1016/j.ijheatmasstransfer.2005.10.005

Nomenclature

G	mass flux
P	pressure
q''	critical heat flux
R	radius
u	velocity
Y	distance between wall and liquid film edge

Greek symbols

α	void fraction
κ	turbulent mixing length constant
ρ	density
τ	viscous stress tensor

Subscripts

c	core region
f	liquid film
m	maximum velocity location
i	inner wall
o	outer wall

Superscript

+	non-dimensional variable

experimental databases available for DNB. However there are few experimental and analytical databases for the dryout because it is only very recent for the dryout models to get highlighted in the PWR analysis. With the introduction of the best-estimation analysis to the design-basis and to the beyond design-basis accident analysis, the dryout phenomena in the core and the steam generator became emphasized for the realistic prediction of transient system response.

General safety analysis codes use the mechanistic models to solve the film dryout phenomena. The mechanistic models for the annular flow dryout have been researched theoretically for several decades. The theoretical processes on the dryout phenomenon were first modeled by Whalley et al. [16] who took into account entrainment of drops, evaporation from the wall film and deposition of drops back onto the film. This was quite successful at predicting the critical heat flux. It was extended by Hewitt and Govan [8] who developed the improved descriptions for entrainment and deposition and allowed for an additional mechanism for entrainment associated with heating suggested by Miloshenko et al. [14].

The theory of film dryout analysis defines that the critical heat flux arises when the liquid film calculated from in the process of evaporation, droplet entrainment and deposition gets dryout. The dryout of film is generally assumed that film thickness becomes zero or small thickness [6]. To determine contribution of dryout, the flow rate of liquid film related to the evaporation process should be estimated accurately, which depends on a geometric characteristics. While only one liquid film is formed along the wall in tube geometry, two films are formed along the inner rod and the outer tube wall in annulus geometry as shown in Fig. 1. Only the inner film in annulus geometry is related to the evaporation process and CHF occurs when the inner film dries out, while the film at outer tube wall, so called cold wall, still exists. This phenomenon is called Cold Wall Effect [15]. Therefore the cold wall effect should be considered for the improvement of film dryout analysis.

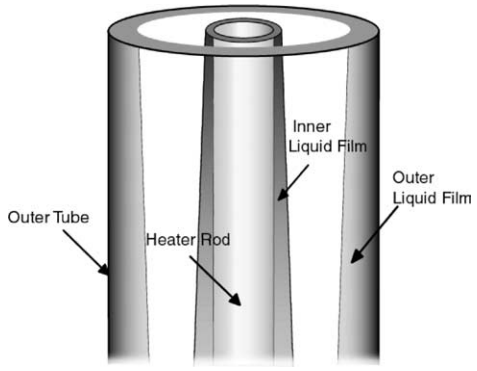

Fig. 1. Liquid film distribution in annulus geometries.

2. Generating film-splitting look-up table using mechanistic model in an annulus geometry

Annular flow in an annulus geometry is characterized as two liquid films flowing along the inner heated rod and the outer unheated wall, whereas the gas flows together with the entrained droplets through the gas core. However, the existence of two films in a calculation cell is not distinguishable in general safety analysis code. This results in the overestimation of dryout in the previous assessments [4]. To compensate such overestimation, a new film-splitting look-up table using mechanistic model was developed, in which the continuous liquid mass flux given by the code is subdivided into two film mass fluxes. One is the liquid mass flux at the outer unheated wall and the other at the inner heated wall [5].

The hydrodynamics module of the code calculates the absolute mass flows for gas, continuous liquid and entrained droplets and also the liquid velocities, which would be used at best in the new film-splitting look-up table. Only the continuous liquid mass phase needs to be split in the code, whereas the mass flows of gas and the entrained droplets are the input for the new model.

In order to develop new film-splitting look-up table mechanically, the assumptions are introduced as follows.

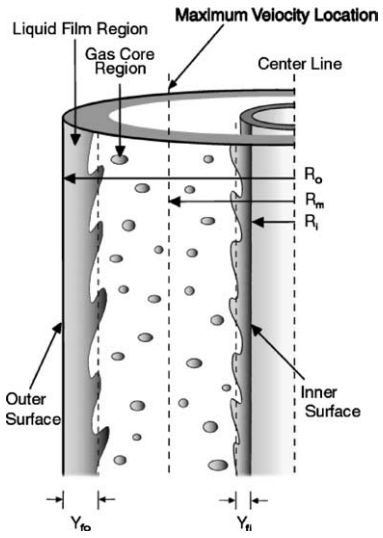

Fig. 2. Schematics of the film-splitting concept.

First, annular flow consists of two continuous film regions and a vapor core region in which continuous vapor and liquid droplets are uniformly mixed. The vapor core region is divided into two regions (outside and inside) according to the location of the maximum velocity plane as shown in Fig. 2 [13]. The velocity profiles in the vapor core regions are then assumed to be the form of a turbulent single-phase universal profile from the law of the wall. The velocities of the liquid films are respectively uniform.

Using the above assumptions, we can get the velocity profiles for outer side as (1) and for inner side as (2):

Core vapor regions

$$u^+_{co} = 2.5 \ln\left(\frac{y}{Y_{fo}}\right) + 5.5 \quad \text{outer side} \tag{1}$$

$$u^+_{ci} = A_i \ln\left(\frac{y}{Y_{fi}}\right) + B_i \quad \text{inner side} \tag{2}$$

The Nikuradse equation is used as the velocity profile in the outside of vapor core. This equation has been used in normal turbulent single phase without an objection. The derived procedure of this equation is as follows [10].

The procedure starts with the assumption of boundary layer near the wall.

The momentum differential equation for the turbulent boundary layer is

$$\overline{u}\frac{\partial \overline{u}}{\partial x} + \overline{v}\frac{\partial \overline{u}}{\partial y} - \frac{\partial}{\partial y}\left[(\nu + \varepsilon_M)\frac{\partial \overline{u}}{\partial y}\right] + \frac{1}{\rho}\frac{d\overline{P}}{dx} = 0 \tag{3}$$

ε_M is dimensionally the same as ν, and the turbulent contribution to diffusion in the y direction can be readily compared with the molecular contribution. In most cases it is found that $\varepsilon_M \gg \nu$ in the fully turbulent region, while $\nu \gg \varepsilon_M$ in the viscous sublayer close to the wall.

The total apparent shear stress, molecular plus turbulent, can be expressed as

$$\frac{\tau}{\rho} = (\nu + \varepsilon_M)\frac{\partial \overline{u}}{\partial y} \tag{4}$$

Substituting this into Eq. (3), we obtain

$$\rho\overline{u}\frac{\partial \overline{u}}{\partial x} + \rho\overline{v}\frac{\partial \overline{u}}{\partial y} - \frac{\partial \tau}{\partial y} + \frac{d\overline{P}}{dx} = 0 \tag{5}$$

In a region relatively close to the wall, the first term is sufficiently smaller than the others that it can be ignored. Under the assumption $\rho\overline{u}(\partial\overline{u}/\partial x) = 0$ and $\overline{u} = \overline{u}(y)$ alone, Eq. (5) becomes an ordinary differential equation, and with $\overline{v} = v_0$, the value of the normal velocity component at the wall surface:

$$\rho v_0 \frac{\partial \overline{u}}{\partial y} - \frac{\partial \tau}{\partial y} + \frac{d\overline{P}}{dx} = 0 \tag{6}$$

This equation can be integrated with respect to y between the limits $\tau = \tau_0$ and $\overline{u} = 0$ at $y = 0$, and corresponding value at any distance y.

$$\frac{\tau}{\tau_0} = 1 + \frac{\rho v_0 \overline{u}}{\tau_0} - + \frac{d\overline{P}}{dx}\frac{y}{\tau_0} \tag{7}$$

A set of non-dimensional variables based on quantities that are significant in the near-wall region is introduced. These are what have been referred to as wall coordinates. First, from the definition of the friction coefficient, a shear velocity or friction velocity, u_τ is defined.

$$u_\tau^2 = \frac{\tau_0}{\rho} \quad \text{or} \quad u_\tau = \sqrt{\frac{\tau_0}{\rho}} \tag{8}$$

u_τ has the dimension of velocity. Employing u_τ as a characteristic velocity, the following non-dimensional variables can be formed.

$$\begin{aligned} u^+ &= \frac{\overline{u}}{u_\tau} \\ y^+ &= \frac{y u_\tau}{\nu} \\ v_0^+ &= \frac{v_0}{u_\tau} \\ p^+ &= \frac{\mu\, d\overline{P}/dx}{\rho^{1/2}\tau_0^{3/2}} \end{aligned} \tag{9}$$

When these are substituted into Eq. (7), we obtain

$$\frac{\tau}{\tau_0} = 1 + v_0^+ u^+ + p^+ y^+ \tag{10}$$

In the region near the wall, Eq. (10) reduces to

$$\frac{\tau}{\tau_0} = 1.0 \tag{11}$$

To obtain the law of the wall, Eq. (4) is integrated under this condition. Thus

$$\frac{\tau_0}{\rho} = (\nu + \varepsilon_M)\frac{\partial \overline{u}}{\partial y} \tag{12}$$

For the fully turbulent region ($\varepsilon_M \gg \nu$)

$$\frac{\tau_0}{\rho} = \varepsilon_M \frac{\partial \overline{u}}{\partial y} \tag{13}$$

Eq. (13) becomes Eq. (15) through introducing the Prandtl mixing-length theory as following equation:

$$\varepsilon_M = l^2\left|\frac{\partial \overline{u}}{\partial y}\right| \tag{14}$$

where l is mixing-length defined as $l = \kappa y$.

$$\frac{\tau_0}{\rho} = l^2\left(\frac{\partial \overline{u}}{\partial y}\right)^2 = \kappa^2 y^2\left(\frac{\partial \overline{u}}{\partial y}\right)^2 \tag{15}$$

The following equation is obtained by introducing the definitions of non-dimensional parameters:

$$\frac{\partial u^+}{\partial y^+} = \frac{1}{\kappa y^+} \tag{16}$$

Then the equation is integrated from the outer edge of the viscous sublayer:

$$\int_{10.8}^{u^+} \mathrm{d}u^+ = \frac{1}{\kappa}\int_{10.8}^{y^+}\frac{\mathrm{d}y^+}{y^+}$$
$$u^+ - 10.8 = \frac{1}{\kappa}\ln\frac{y^+}{10.8} \tag{17}$$

Setting $\kappa = 0.41$ and rearranging, the logarithmic equation that is generally called the law of the wall is obtained

$$u^+ = 2.44\ln y^+ + 5.0 \tag{18}$$

However the above equation is not valid for tube because the shear stress is not independent of r. Some modification is necessary. Generally, the following modified equation is used in tube geometry.

$$u^+ = 2.5\ln y^+ + 5.5 \tag{19}$$

Here y^+ is the non-dimensional distance from the tube wall.

In the case of liquid film existence, y^+ is generally defined as the ratio of distance from the tube wall to film thickness.

There are several equations based on theoretical approaches for inside of an annulus geometry but it was proven that these approaches are not matched with experimental data [12]. Instead, many researchers have suggested fitting parameters with experimental data [11].

The coefficients A_i and B_i of inner side velocity profiles have been proposed by many researchers. Ballow et al. produced these values by fitting with several experimental data banks [1]. In this study, the Ballow's correlation shown as Eq. (20) is used because of the wide application range. The range of experimental data that is used for developing this correlation is given as Table 1. This range is applicable to most of annulus CHF tests.

Table 1
Experimental condition used for barrow correlation

Parameter	Range
Fluid	Air, water
R_i/R_o	0.065–0.562
Reynolds	9000.0–320,000.0

$$A_i = 2.7\left(\frac{R_i}{R_o}\right)^{0.353}, \quad B_i = 3.6\left(\frac{R_i}{R_o}\right)^{-0.439} \tag{20}$$

Calculation procedures of the new film-splitting model are as follows:

1. Guess the maximum velocity location (R_m).
2. Guess the outside film thickness (Y_{fo}).
3. Calculate the liquid fraction of outside film as

$$\alpha_{fo} = \frac{R_o^2 - (R_o - Y_{fo})^2}{R_o^2 - R_i^2} \tag{21}$$

4. Guess the inside film thickness (Y_{fi}).
5. Calculate the ratio of the outside interfacial shear stress to that of inside. This ratio is calculated from the pressure drop in each side.

   The outside interfacial shear stress is derived from the outside pressure drop:

$$-\left(\frac{\mathrm{d}P}{\mathrm{d}z}F\right)_{i_o} = \frac{A_{i_o}\tau_{i_o}}{A_i\,\mathrm{d}z} = \frac{\pi(R_o - Y_{fo})\tau_{i_o}}{\frac{\pi}{4}\left[(R_o - Y_{fo})^2 - R_m^2\right]} = \frac{4(R_o - Y_{fo})\tau_{i_o}}{(R_o - Y_{fo})^2 - R_m^2} \tag{22}$$

   Similarly, the inside shear stress is

$$-\left(\frac{\mathrm{d}P}{\mathrm{d}z}F\right)_{i_i} = \frac{4(R_i + Y_{fi})\tau_{i_i}}{R_m^2 - (R_i + Y_{fi})^2} \tag{23}$$

   The pressure drops of both sides should be equal. Therefore

$$-\left(\frac{\mathrm{d}P}{\mathrm{d}z}F\right)_{i_o} = -\left(\frac{\mathrm{d}P}{\mathrm{d}z}F\right)_{i_i}$$
$$\frac{4(R_o - Y_{fo})\tau_{i_o}}{(R_o - Y_{fo})^2 - R_m^2} = \frac{4(R_i + Y_{fi})\tau_{i_i}}{R_m^2 - (R_i + Y_{fi})^2} \tag{24}$$

   Finally, the ratio of the interfacial shear stress in each side is obtained as follows:

$$\frac{\tau_{i_o}}{\tau_{i_i}} = \frac{R_i + Y_{fi}}{R_o - Y_{fo}}\frac{(R_o - Y_{fo})^2 - R_m^2}{R_m^2 - (R_i + Y_{fi})^2} \tag{25}$$

6. Calculate the liquid fraction of inside film

$$\alpha_{fi} = \frac{(R_i + Y_{fi})^2 - R_i^2}{R_o^2 - R_i^2} \tag{26}$$

7. Find Y_{fi} that satisfies the continuity of gas core velocity at R_m

$$u_{co}\left(\frac{R_o - R_m}{Y_{fo}}\right) = u_{ci}\left(\frac{R_m - R_i}{Y_{fi}}\right) \tag{27}$$

$$\sqrt{\frac{\tau_{i_o}}{\rho}}u_{co}^+\left(\frac{R_o - R_m}{Y_{fo}}\right) = \sqrt{\frac{\tau_{i_i}}{\rho}}u_{ci}^+\left(\frac{R_m - R_i}{Y_{fi}}\right)$$
$$\sqrt{\frac{\tau_{i_o}}{\tau_{i_i}}}\left[2.5\ln\left(\frac{R_o - R_m}{Y_{fo}}\right) + 5.5\right] = A_i\ln\left(\frac{R_m - R_i}{Y_{fi}}\right) + B_i \tag{28}$$

8. Determine Y_{fo} that satisfies the condition that the sum of outside and inside liquid fraction is equal to liquid fraction calculated from the code

$$\alpha_{\mathrm{fo}} + \alpha_{\mathrm{fi}} = \alpha_{\mathrm{f,Code}} \tag{29}$$

9. To determine R_{m}, repeat step 1 to step 8 until the continuity of the eddy diffusivity at R_{m} is satisfied. The inner and outer liquid film thickness and liquid fractions satisfying this condition are then determined

$$\varepsilon_{M_{\mathrm{o}}} = \varepsilon_{M_{\mathrm{i}}}, \quad \kappa_{\mathrm{o}} y_{\mathrm{o},R_{\mathrm{m}}} \sqrt{\frac{\tau_{\mathrm{i_o}}}{\rho}} = \kappa_{\mathrm{i}} y_{\mathrm{i},R_{\mathrm{m}}} \sqrt{\frac{\tau_{\mathrm{i_i}}}{\rho}}$$
$$\frac{1}{2.5}(R_{\mathrm{o}} - R_{\mathrm{m}})\sqrt{\frac{\tau_{\mathrm{i_o}}}{\rho}} = \frac{1}{A_{\mathrm{i}}}(R_{\mathrm{m}} - R_{\mathrm{i}})\sqrt{\frac{\tau_{\mathrm{i_i}}}{\rho}} \tag{30}$$

The ratio of outside wall shear stress to that at inside wall is also obtained from pressure drop

$$-\left(\frac{\mathrm{d}P}{\mathrm{d}z}F\right)_{w_{\mathrm{o}}} = -\left(\frac{\mathrm{d}P}{\mathrm{d}z}F\right)_{w_{\mathrm{i}}}$$
$$\frac{4R_{\mathrm{o}}\tau_{\mathrm{i_o}}}{R_{\mathrm{o}}^2 - R_{\mathrm{m}}^2} = \frac{4R_{\mathrm{i}}\tau_{\mathrm{i_i}}}{R_{\mathrm{m}}^2 - R_{\mathrm{i}}^2}$$
$$\frac{\tau_{R_{\mathrm{o}}}}{\tau_{R_{\mathrm{i}}}} = \frac{R_{\mathrm{i}}}{R_{\mathrm{o}}}\frac{R_{\mathrm{o}}^2 - R_{\mathrm{m}}^2}{R_{\mathrm{m}}^2 - R_{\mathrm{i}}^2} \tag{31}$$

The following relationship is obtained from the definition of wall shear stress. Here, the Blausius correlation is used in order to determine the wall friction factor at both sides [10]:

$$\frac{\tau_{R_{\mathrm{o}}}}{\tau_{R_{\mathrm{i}}}} = \frac{f_{\mathrm{fo}}\frac{\rho_{\mathrm{L}}u_{\mathrm{fo}}^2}{2}}{f_{\mathrm{fi}}\frac{\rho_{\mathrm{L}}u_{\mathrm{fi}}^2}{2}} \tag{32}$$

Introducing the Blausius correlation as $f = 0.078\,Re^{-0.25}$

$$\frac{\tau_{R_{\mathrm{o}}}}{\tau_{R_{\mathrm{i}}}} = \frac{f_{\mathrm{fo}}\rho_{\mathrm{L}}u_{\mathrm{fo}}^2/2}{f_{\mathrm{fi}}\rho_{\mathrm{L}}u_{\mathrm{fi}}^2/2} = \frac{Re_{\mathrm{fo}}^{-0.25}u_{\mathrm{fo}}^2}{Re_{\mathrm{fi}}^{-0.25}u_{\mathrm{fi}}^2} = \frac{\alpha_{\mathrm{fo}}^{-0.25}u_{\mathrm{fo}}^{1.75}}{\alpha_{\mathrm{fi}}^{-0.25}u_{\mathrm{fi}}^{1.75}} \tag{33}$$

From above equation, the ratio of outer film velocity to inside film velocity becomes

$$\frac{u_{\mathrm{fo}}}{u_{\mathrm{fi}}} = \left(\frac{\alpha_{\mathrm{fo}}}{\alpha_{\mathrm{fi}}}\right)^{1/7}\left(\frac{\tau_{R_{\mathrm{o}}}}{\tau_{R_{\mathrm{i}}}}\right)^{1/1.75} \tag{34}$$

Finally, the ratio of each side liquid film mass fluxes to total liquid film mass flux is calculated using the liquid fractions in each side and the liquid film velocity ratio

$$\frac{G_{\mathrm{fo}}}{G_{\mathrm{fi}}} = \left(\frac{\alpha_{\mathrm{fo}}}{\alpha_{\mathrm{fi}}}\right)\left(\frac{u_{\mathrm{fo}}}{u_{\mathrm{fi}}}\right) \tag{35}$$
$$\frac{G_{\mathrm{fo}}}{G_{\mathrm{f}}} = \frac{\frac{G_{\mathrm{fo}}}{G_{\mathrm{fi}}}}{1 + \frac{G_{\mathrm{fo}}}{G_{\mathrm{fi}}}} \tag{36}$$

The above process is described in Fig. 3.

The film-splitting table was generated using the pilot code to cover wide ranges of ratio of inner radius to outer radius and continuous liquid fraction. The applicable ranges of the look-up table are as shown in Table 2.

The ratio of outer liquid mass flow rate to total liquid mass flow rate in this table is expressed in Fig. 4.

Table 2
Application range of film-splitting look-up table

Parameter	Range
$R_{\mathrm{i}}/R_{\mathrm{o}}$	0.1–0.8
Continuous liquid fraction	0.0001–0.3

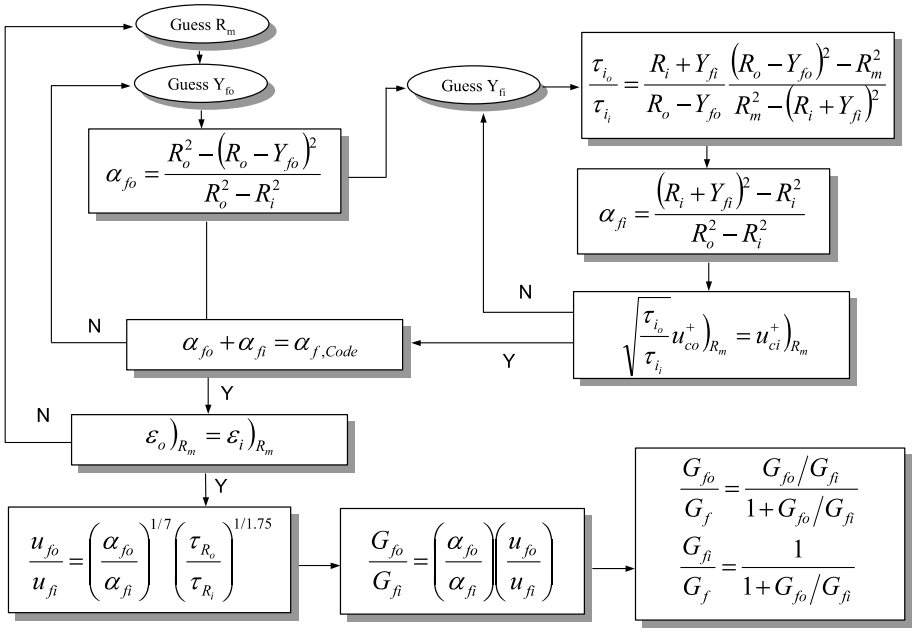

Fig. 3. Process of film-splitting model.

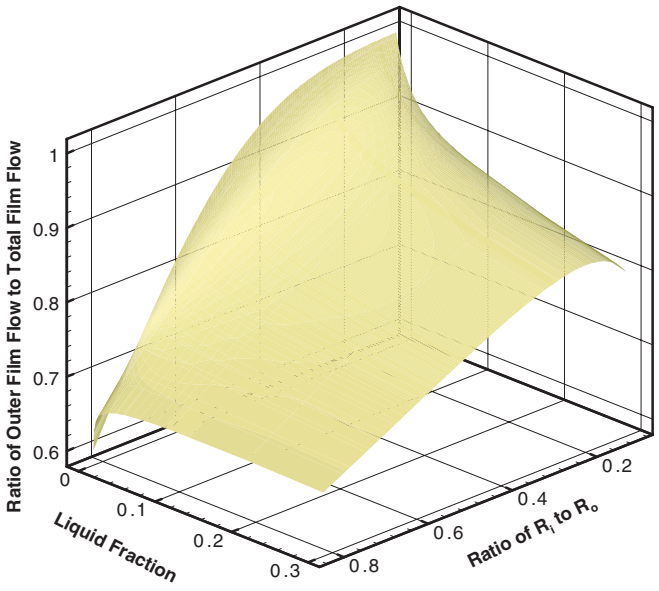

Fig. 4. G_{fo}/G_f value in the new film-splitting table.

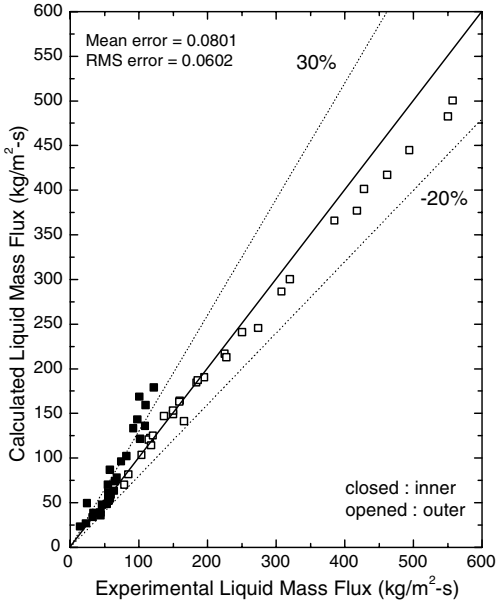

Fig. 5. Comparison of outer and inner liquid mass fluxes.

3. Assessment of mechanistic film-splitting model look-up table

Based on the new film-splitting model, a look-up table has been developed and examined for accuracy. In order to examine the effectiveness of the new film-splitting look-up table, Wurtz' experimental data [17] has been assessed. Test 17/26L was selected for the assessment, which are the steam-water annular flow tests in the annulus geometry with adiabatic conditions. The annulus geometry has an outer diameter of 0.026 m and inner rod's diameter of 0.017 m. The pressure ranges from 30 to 90 bars and the quality ranges from 20% to 60%. In the tests, the flow rate and thickness of the liquid films were measured by varying the inlet mass flow and the exit quality.

From the look-up table assessment, it was found that the outside film flows were slightly underestimated and the inner flow rates were overestimated as shown in Fig. 5. Since the pilot code simply splits the continuous liquid flow into the inner and outer flow, even the slight underestimation of the outer flow may result in a larger deviation of the inner flow.

The outer film flow rate is larger than inner film flow rate in most of the cases, and this is due to the velocity distribution in the vapor core. The maximum velocity plane in the vapor core is shifted to inner side. This phenomenon is understood easily using the example of simple laminar case shown in Fig. 6. It was reported that the maximum velocity plane is shifted to inner side as the R_i/R_o decreases [3]. The average inner velocity is greater than the average outer velocity in the vapor core and this difference of both sides causes the difference of film thickness that the inner film thickness is thinner than outer film thickness. This difference of film thickness results in the difference of liquid fraction and mass flux of both liquid films.

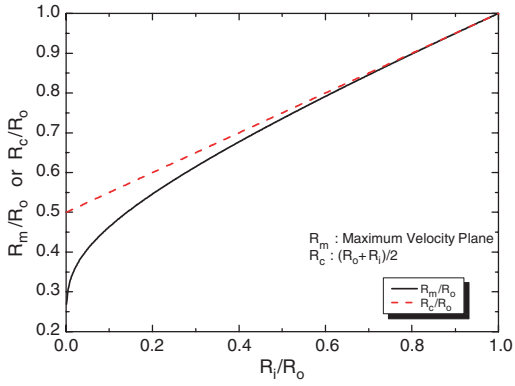

Fig. 6. Location of maximum velocity plane for laminar flow.

This film-splitting look-up table should be used in CHF calculation. Thus the table has been assessed indirectly using several CHF data including annulus geometry. Fig. 7 is plots of the experimental data versus calculation results for CHF experiments. While Janssen's experiment and Becker's experiment are performed at uniform heating condition [9,2], KAERI test have both uniform and non-uniform heater shaping cosine power [7]. Although some data having large deviation are shown in the non-uniform heating KAERI data, most of the results including non-uniform shape are estimated well in RMS error of 0.12. Also these results represent that results including film-splitting model gives better prediction than results without this model (open data).

4. Conclusion

To improve accuracy of film dryout, it is very important to estimate liquid film flow rate accurately. The liquid film

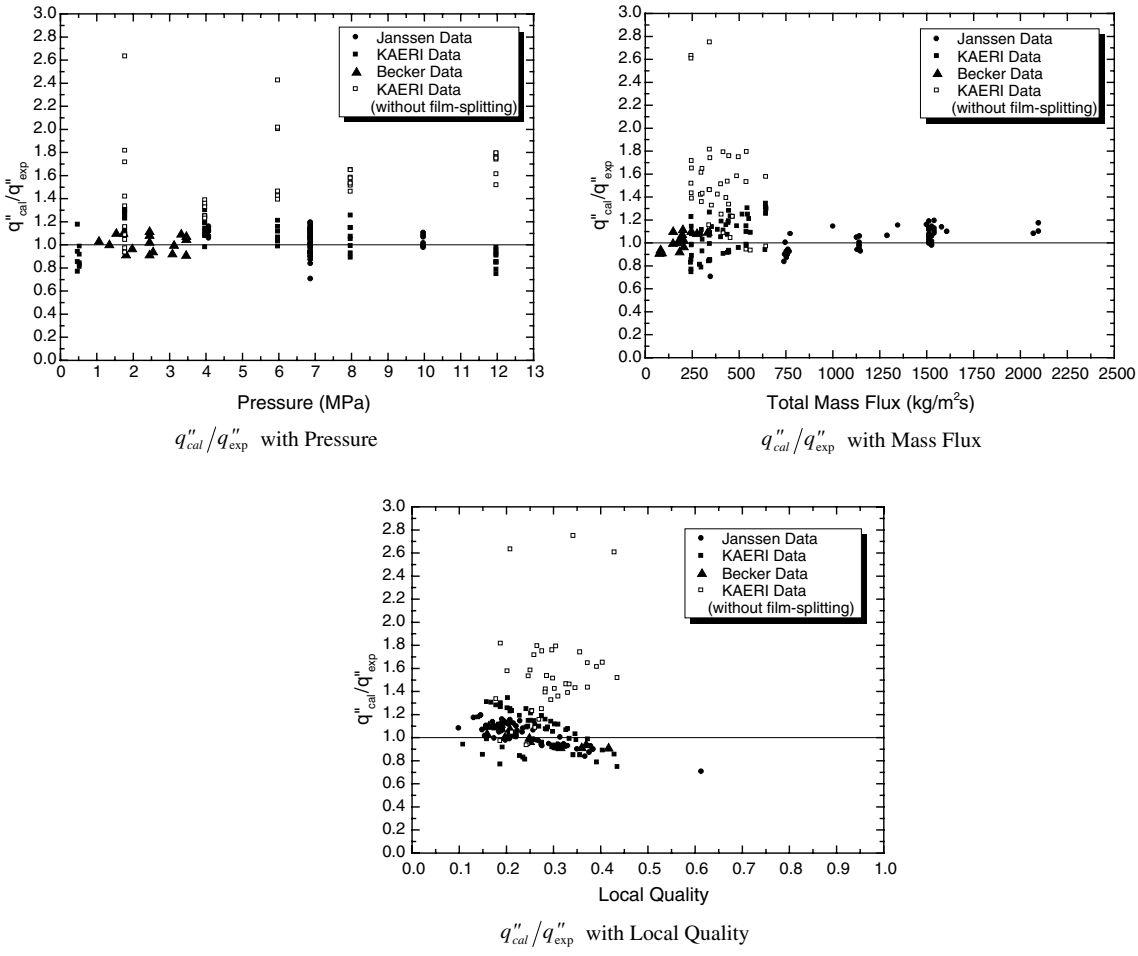

$q''_{cal}/q''_{\exp}$ with Pressure

$q''_{cal}/q''_{\exp}$ with Mass Flux

$q''_{cal}/q''_{\exp}$ with Local Quality

Fig. 7. Annulus geometry dryout assessments.

flow rate related an evaporation process should be estimated accurately and depends on a geometric characteristic because all amount of liquid flow in the tube geometry are evaporated but only some part of liquid is evaporated in the annulus geometry. Here, new mechanistic film-splitting model for annulus geometry is necessary because of cold wall effect. Mechanistic film-splitting in annulus geometry is modeled in the code by using a film-splitting look-up table. The look-up table was generated using the mechanistic film-splitting model in various flow conditions. And this look-up table was assessed using Wurtz experimental data and several annulus CHF tests. These assessments showed reasonably good results estimated in RMS error of 0.12.

References

[1] H. Barrow et al., The similarity hypothesis applied to turbulent flow in an annulus, Int. J. Heat Mass Transfer 8 (1965) 1499–1505.

[2] K.M. Becker et al., Burnout data for flow of boiling water in vertical round ducts, Annuli and Rod Clusters, AE-177, 1965.

[3] J.A. Brighton et al., Fully developed turbulent flow in annuli, J. Basic Eng. (1964) 835–844.

[4] J.H. Chun et al., Assessment of MARS 1.4 dryout model using KAERI annulus CHF test, in: Proceeding of KSME Conference, 1999, pp. 607–613.

[5] J.H. Chun et al., MARS mechanistic film-splitting and dryout model in annulus geometry, in: Proceeding of the Korean Nuclear Society Spring Meeting, 2001.

[6] J.H. Chun et al., Development of the critical film thickness correlation for and advanced annular film mechanistic dryout model applicable to MARS code, Nucl. Eng. Des. 223 (2003) 315–328.

[7] S.Y. Chun, Effect of pressure on critical heat flux in vertical annulus flow channel under low flow condition, in: Proceeding of NTHAS98, 1998, pp. 342–347.

[8] G.F. Hewitt, A.H. Govan, Phenomenological modeling of non-equilibrium flows with phase change, Int. J. Heat Mass Transfer 33 (2) (1990) 229–242.

[9] E. Janssen et al., Burnout conditions for single rod in annular geometry, Water at 600–1400 Psia GEAP-3899, 1963.

[10] W.M. Kays, M.E. Crawford, Convective Heat and Mass Transfer, McGraw-Hill, 1993.

[11] J.G. Knudsen, D.L. Katz, Fluid Dynamics and Heat Transfer, McGraw-Hill, New York, 1958.

[12] S. Levy et al., Turbulent flow in an annulus, J. Heat Transfer Trans ASME 89 (1967) 25–31.

[13] S. Levy et al., Analysis of annular liquid–gas flow with entrainment concurrent vertical flow in an annulus, EPRI Report NP-1563, 1980.

[14] V.I. Miloshenko et al., Burnout and distribution of liquid in evaporative channels of various lengths, Int. J. Multiphase Flow 15 (3) (1989) 393–401.

[15] L.S. Tong, J. Weisman, Thermal Analysis of Pressurized Water Reactors, American Nuclear Society, USA, 1979.
[16] P.B. Whalley et al., The calculation of critical heat flux in forced convection boiling, in: Proceeding of 5th International Heat Transfer Conference, Tokyo, vol. 4, 1974, pp. 290–294.
[17] J. Wurtz et al., An experimental and theoretical investigation of annular steam–water flow in tubes and annuli at 30–90 bar, Riso Report, No. 372, 1978.